

# Spin-defect characteristics of single sulfur vacancies in monolayer MoS<sub>2</sub>

A. Hötger,<sup>1</sup> T. Amit,<sup>2</sup> J. Klein,<sup>3</sup> K. Barthelmi,<sup>1</sup> T. Pelini,<sup>4</sup> A. Delhomme,<sup>4</sup> S. Rey,<sup>5</sup>

M. Potemski,<sup>4,6</sup> C. Faugeras,<sup>4</sup> G. Cohen,<sup>2</sup> D. Hernangómez-Pérez,<sup>2</sup> T. Taniguchi,<sup>7</sup> K.

Watanabe,<sup>8</sup> C. Kastl,<sup>1</sup> J.J. Finley,<sup>1</sup> S. Refaely-Abramson,<sup>2</sup> A.W. Holleitner,<sup>1</sup> and A.V. Stier<sup>1</sup>

<sup>1</sup>Walter Schottky Institute and Physics Department, TU Munich, 85748 Garching, Germany.

<sup>2</sup>Department of Molecular Chemistry and Materials Science, Weizmann Institute of Science, Rehovot, Israel.

<sup>3</sup>Department of Materials Science and Engineering,

Massachusetts Institute of Technology, Cambridge, Massachusetts 02139, USA

<sup>4</sup>Laboratoire National des Champs Magnétiques Intenses,

CNRS-UGA-UPS-INSA-EMFL, 38042 Grenoble, France.

<sup>5</sup>Department of Photonics Engineering, Technical University of Denmark, 2800 Kgs. Lyngby, Denmark.

<sup>6</sup>Institute of Experimental Physics, Faculty of Physics,

University of Warsaw, 02-093 Warszawa, Poland

<sup>7</sup>International Center for Materials Nanoarchitectonics,

National Institute for Materials Science, 1-1 Namiki, Tsukuba 305-0044, Japan.

<sup>8</sup>Research Center for Functional Materials, National Institute for Materials Science, 1-1 Namiki, Tsukuba 305-0044, Japan.

(Dated: May 23, 2022)

Single spin defects in 2D transition-metal dichalcogenides are natural spin-photon interfaces for quantum applications. Here we report high-field magneto-photoluminescence spectroscopy from three emission lines (Q1, Q2 and Q\*) of He-ion induced sulfur vacancies in monolayer MoS<sub>2</sub>. Analysis of the asymmetric PL lineshapes in combination with the diamagnetic shift of Q1 and Q2 yields a consistent picture of localized emitters with a wavefunction extent of  $\sim 3.5$  nm. The distinct valley-Zeeman splitting in out-of-plane  $B$ -fields and the brightening of dark states through in-plane  $B$ -fields necessitates spin-valley selectivity of the defect states and lifted spin-degeneracy at zero field. Comparing our results to ab-initio calculations identifies the nature of Q1 and Q2 and suggests that Q\* is the emission from a chemically functionalized defect. Analysis of the optical degree of circular polarization reveals that the Fermi level is a parameter that enables the tunability of the emitter. These results show that defects in 2D semiconductors may be utilized for quantum technologies.

## I. INTRODUCTION

Spin-defects in host crystals can be fundamental building blocks for quantum technologies, such as computing, sensing or communication[1–3]. For instance, color centers in diamond have been investigated since the early 1980s, of which the nitrogen vacancy center (NV) is the most prominent example[4, 5]. In this defect, the crystal field splitting lifts the ground state spin degeneracy and provides the required unique quantum degree of freedom to form an addressable two-level system[6–9]. Additionally, NV centers are single photon sources[10–12] and therefore constitute excellent building blocks for future quantum photonic circuits. However, a key prerequisite for such applications is the ability to position defects deterministically. This is a challenge for defects in 3D crystals, such as single NV centers, as they can be positioned either vertically or laterally with high precision, but not both simultaneously[13–16]. This disadvantage can be overcome by creating optically addressable spin-defects in 2D host crystals. Localized single photon emission in 2D materials was first discovered in monolayer WSe<sub>2</sub>, a prototypical member of the semiconducting 2D transition metal dichalcogenides (TMDs)[17–21]. Subsequently, single photon emitters were discovered in hexagonal boron nitride (hBN)[22]. Contrasted with hBN, TMDs have strong light-matter coupling[23] and locked spin-valley physics[24], which provides a nat-

ural spin-photon interface. The 2D semiconducting host crystal has further enabled new possibilities to engineer and manipulate these defects[18, 25–27], which led to further advances in quantum devices, such as quantum light emitting diodes[28–30].

First approaches for the deterministic creation of quantum emitters in 2D materials made use of strain potentials, for instance induced by a textured substrate[31–37]. This results in a local bandstructure modulation in the host crystal, limited by the bending radius of the material, yet the latter approach intrinsically lacks reproducibility. Furthermore, the confining potential often breaks crystal symmetries, leading to the loss of valley optical selection rules. A higher degree of spatial resolution and reproducibility can be achieved by using the accuracy of electron-beam or focused ion beam irradiation[38–42]. Specifically, He-ions can be precisely focused and create optically active point defects in monolayer MoS<sub>2</sub> [40] with a precision better than 10 nm. [43] In photoluminescence (PL) spectroscopy, spectrally narrow emission lines appear about 200 meV red-shifted from the neutral exciton of He-ion irradiated MoS<sub>2</sub> [40]. Second order correlation measurements unambiguously showed single photon emission from single He-ion irradiation sites, which in turn could be related to the generated point defects[44, 45]. A specific advantage is that these defects can be implanted into more complex, electronic device heterostructures, allowing for the electrical

control of quantum emission[27].

The microscopic origin of various localized emission centers is currently a matter of debate. One specific defect complex, which is predominant in He-ion irradiated MoS<sub>2</sub>, is the chalcogen vacancy, where one sulfur atom has been removed from the host lattice[43]. Sub-gap quantum emission from this defect[46] was suggested to originate from a relaxation cascade where an optical interband excitation creates a bound electron-hole pair that subsequently localizes into the defect and radiatively recombines[47]. However, pristine defect states have been predicted to be essentially spin degenerate[46, 48]. Moreover, other relaxation pathways, such as defect-to-band transitions are in principle possible, and, due to the strong spin-orbit interaction in the host MoS<sub>2</sub>, considerations with respect to spin-valley physics have yet to be taken into account. In this manuscript, we investigate three distinct emission lines of He-ion induced sulfur vacancies created in monolayer MoS<sub>2</sub> by high-field magneto-optical spectroscopy, which has previously been shown to be an important tool to investigate the excitonic spin-valley physics in 2D TMDs[49–51]. We identify the bands involved in the optical quantum emission and show that an energy dependent degree of hybridization between atom-like defect states and the MoS<sub>2</sub> bandstructure leads to varying degree of valley selectivity for the distinct electron-hole transitions. Our results display that sulfur vacancies in monolayer MoS<sub>2</sub> are spin-defects that can be tailored to specific quantum applications.

## II. RESULTS

### A. Photoluminescence from sulfur vacancies in monolayer MoS<sub>2</sub>

The left hand side of Fig. 1a shows the schematic of the sample under investigation. A monolayer MoS<sub>2</sub> is encapsulated in hBN, fabricated by standard dry viscoelastic stamping methods (see Methods for details). Subsequently, a focused He-ion beam is scanned across the sample, creating predominantly sulfur vacancies in the MoS<sub>2</sub>[43]. Our sample is He-ion irradiated with a pitch of  $\sim 2 \mu\text{m}$ , which allows us to selectively investigate individual irradiated locations (see Supplementary information Fig. S1 a). Typical defect PL spectra at 1.7 K and zero magnetic field are shown in Fig. 1b. The dominant feature at 1.75 eV, labeled Q1, has previously been identified as a single photon emitter[44, 45] associated with an unpassivated sulfur vacancy[47]. In this manuscript, we discuss only those locations which contained a single Q1 line, generally the case for the sample under investigation. The low energy tail of Q1 is attributed to the coupling of a localized state to acoustic phonons in MoS<sub>2</sub>. Analysis of the lineshape with an independent boson model allowed the determination of the effective Bohr radius of this localized state to be  $\approx 2\text{-}3 \text{ nm}$ [40]. A

weak secondary feature about 30 meV red-shifted from the zero phonon line (ZPL) of Q1, can be assigned to a phonon replica due to a local phonon mode (LPM) of this defect center[45]. Emission line Q2 forms in a distinct energy band  $\approx 75 \text{ meV}$  red-shifted from Q1, while emission line Q\* appears  $\approx 50 \text{ meV}$  blue-shifted. Both lines generally appear fainter as compared to Q1, while the lineshape of all features are similar. The statistical appearance of all emission lines investigated throughout the sample clearly indicates these three inhomogeneously broadened, yet distinct, emission bands (see Supplementary Information Fig. S1 b). Our zero B-field spectroscopy therefore establishes the observed emission lines to originate from localized defect centers. This is consistent with predictions of the electron wavefunction of a defect state associated with a sulfur vacancy (see Supplementary Information Fig. S8). As sketched in Fig. 1c and discussed in detail below, we unambiguously identify Q1 as an excitonic transition predominantly between defect induced states (cD1/cD2  $\leftrightarrow$  vD) at the  $\Gamma$  point, with significant hybridization across the Brillouin zone and specifically at the  $K/K'$  points[46]. This spread in momentum-space originates from the localized character of the sulfur vacancy, as shown by the calculated wavefunction distributions associated with the electronic defect levels cD1, cD2 and vD (see Supplementary Information, Figure S8). The wavefunctions are primarily composed of transition metal d-orbitals and therefore contain the spin-valley physics of monolayer MoS<sub>2</sub> throughout the Brillouin zone[46]. For the energetically lower lying emission Q2, we identify the superposition of transitions between both spin up/down defect induced conduction band states (cD1) and the MoS<sub>2</sub> valence band (VB) at the  $K/K'$ -points in the Brillouin zone. Although Q2 is also excitonic, the transitions are confined to the  $K/K'$ -points. We further demonstrate that Q\* originates from a chemically functionalized sulfur vacancy and the emission is of character Q2. One of the central aspects of this manuscript is the observation of the valley dichroism of all emission lines through the valley Zeeman splitting and optical degree of circular polarization (DCP) in high magnetic fields. We note that valley selectivity stems from contributions at the  $K/K'$ -points to the excitonic transitions, which we probe via circular polarization resolved magneto-spectroscopy. As an example, the DCP of Q1 and Q2 are shown in 1d, which, for Q1 reveals essentially no polarization in the B-field range below 15 T, and a rapid rise of the DCP, tending towards unity at the highest fields. Q2 polarizes already at low fields and saturates at  $\approx 80\%$  for fields above 15 T. The observation that these emission lines show valley dichroism at finite magnetic field necessitates the lifting of the spin degeneracy, and we further proof in detail below that the spin degeneracy of the defect states in the  $K/K'$  valleys is already lifted at zero magnetic field. Thus, the sulfur vacancy in MoS<sub>2</sub> can be considered as a spin defect.

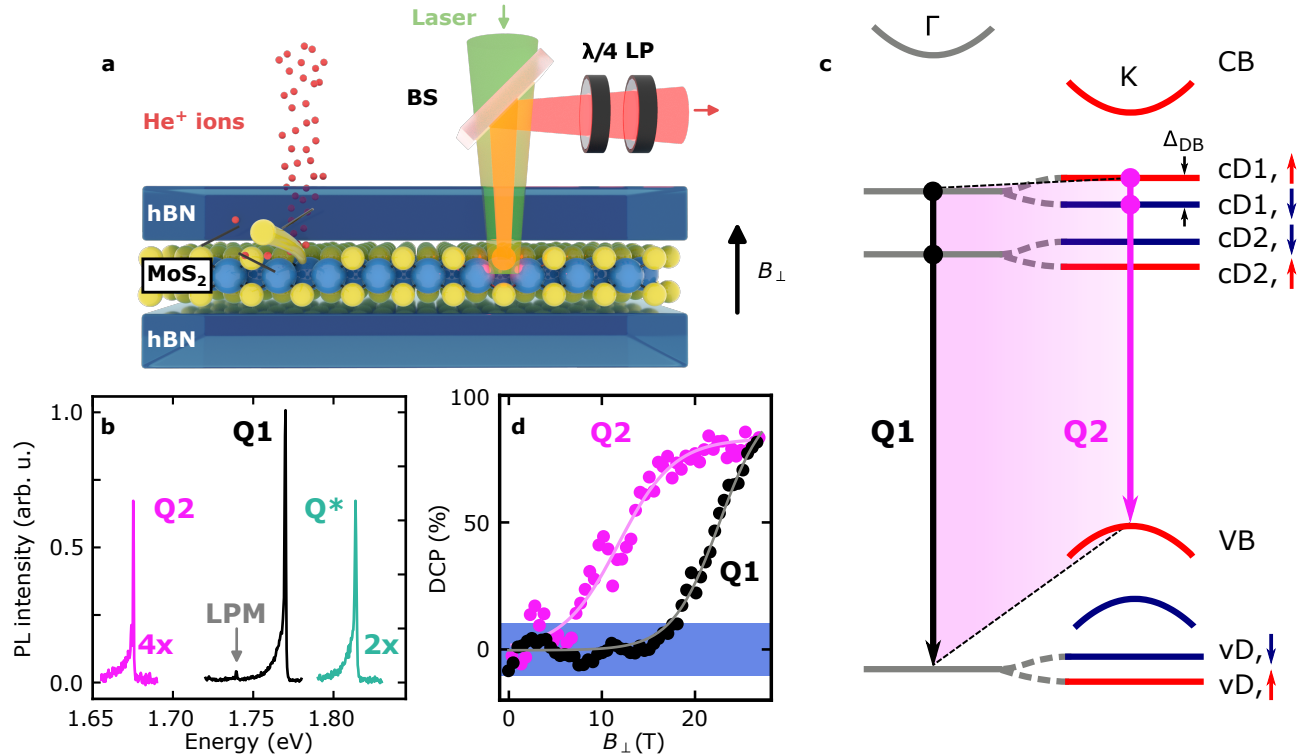


**Figure 1 | Defect luminescence of He-ion irradiated monolayer  $\text{MoS}_2$ .** a) Sketch of the monolayer  $\text{MoS}_2$  encapsulated in hBN illustrating the He-ion irradiation and the out-of-plane magneto-spectroscopy scheme. b) Typical low-temperature photoluminescence (PL) spectra of the quantum emission Q1, Q2, and  $\text{Q}^*$  and the local phonon mode (LPM) of Q1. c) Illustration of the  $\text{MoS}_2$  bandstructure at the  $K$  and  $\Gamma$  valleys including the defect states of a sulfur vacancy. The modified bandstructure shows flat defect-related levels vD, cD2 and cD1. The defect states are doubly degenerate at the  $\Gamma$  point, whereas a small spin splitting is expected in the  $K/K'$  valley. d) Degree of circular polarization (DCP) versus  $B_\perp$  for Q1 and Q2. The blue shaded area highlights the  $\pm 10\%$  experimental uncertainty. The oscillations in the DCP below  $\approx 15$  T are predominantly due to fringe field induced Faraday rotation in the low temperature objective. The data is fitted with Eq.1 (solid lines).

### B. Out-of-plane magnetic field measurements on defects in $\text{MoS}_2$

In order to investigate the nature of the observed emission bands, we employ magneto-PL spectroscopy. Figure 1a shows the schematic of the experiment, where the magnetic field  $B_\perp$  up to 27 T is applied perpendicular to the 2D sample plane and parallel to the optical beam path (Faraday geometry). The sample was mounted in a He-exchange gas cryostat with a bath temperature of  $T = 4.2$  K. The sample was excited with a linearly polarized continuous wave (CW) laser at a wavelength of 515 nm and power of  $\sim 10$   $\mu\text{W}$ , focused to a beam spot of  $\sim 1 \mu\text{m}$ . The linear polarization excites interband transitions in both  $K/K'$  valleys of the host  $\text{MoS}_2$ . At each positive magnetic field, we probe the circular dichroism by detecting the PL for  $\sigma^-$  and  $\sigma^+$  polarization, which we calibrate with the well known valley Zeeman splitting of the neutral exciton in  $\text{MoS}_2$  (Supplementary Information Fig. S2). As such, we minimize the impact of positional sample drift with respect to the beam path

in very high magnetic fields. From the faint appearance of the negatively charged trion in the PL spectra and the value of the valley Zeeman magnetic moment for the neutral exciton ( $\mu_\perp = -2.6 \mu_B$ ), we conclude that our  $\text{MoS}_2$  crystal is weakly electron doped  $n \approx 5 \times 10^{11} \text{ cm}^{-2}$ [52]. Figure 2a depicts typical polarization resolved PL spectra of Q1 and the LPM at 0 T. Unlike strain induced quantum emitters in monolayer TMDs[31, 35, 53], the He-ion-induced defects show no valley dichroism at zero magnetic field[47]. This is expected for the  $C_{3v}$  symmetry of an unperturbed sulfur vacancy with defect-to-defect transitions at the  $\Gamma$ -point (see Fig. 1d)[46, 48]. The left (right) panel of Fig. 2b shows the normalized PL of Q1 versus  $B_\perp$  for  $\sigma^-$  ( $\sigma^+$ ) polarized detection. The position of the ZPL exhibits a monotonic blue-shift with increasing magnetic field for both polarizations. We plot the PL peak position in Figure 2c and find that the average peak position for  $\sigma^+$  and  $\sigma^-$  detection  $\frac{1}{2}(E_{\sigma+} + E_{\sigma-})$  can be fitted with a quadratic function ( $\sim B_\perp^2$ ) with a prefactor of  $\sigma = 1.0 \pm 0.1 \text{ meV T}^{-2}$ . The quadratic-in- $B_\perp$  blueshift is consistent

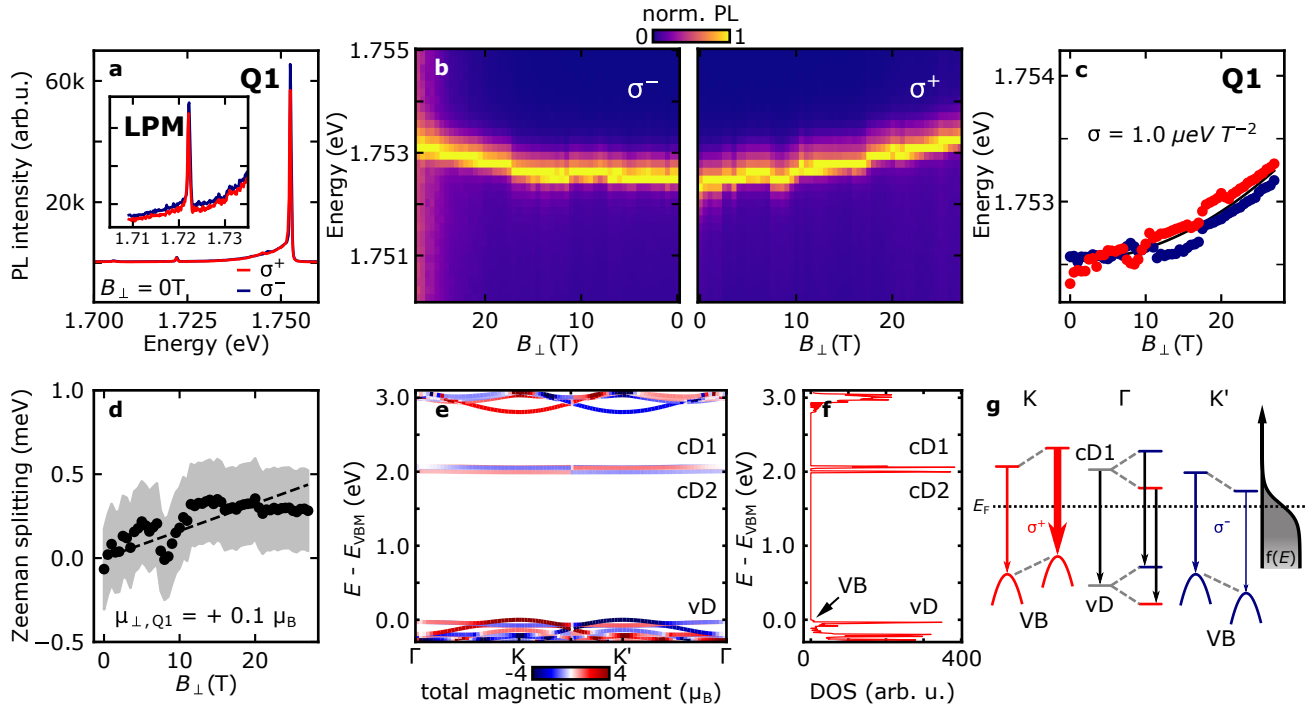


**Figure 2 | Out-of-plane magnetic field  $B_{\perp}$  dependent photoluminescence of defect luminescence Q1.** a) Low-temperature photoluminescence (PL) spectra of defect luminescence Q1 at zero out-of-plane magnetic field ( $B_{\perp}$ ) for  $\sigma^+$  (red) and  $\sigma^-$  (blue) polarized detection. The zero-phonon line (ZPL) of Q1 occurs at 1.752 eV with a red-shifted (30 meV) local phonon mode (LPM, see inset). b) PL versus  $B_{\perp}$  for Q1. The left (right) panel shows the  $\sigma^-$  ( $\sigma^+$ ) polarized signal. The spectra were normalized to their maximum intensity. c) The fitted position of the ZPL of Q1 shows a diamagnetic shift of  $1.0 \pm 0.1 \mu\text{eV T}^{-2}$ . d) Valley Zeeman splitting of Q1 versus  $B_{\perp}$ . The black dashed line shows the expected Zeeman splitting for a transition from cD1 to vD with a calculated Zeeman splitting of  $\mu_{\perp,Q1} = +0.1 \pm 0.1 \mu_B$ . e) Bandstructure of MoS<sub>2</sub> with a periodic sulfur-vacancy extracted from DFT calculations. The color code denotes the total magnetic moment at each k-point. f) Density of states (DOS) plot of the Brillouin zone, showing energetically narrow densities at the defect levels. g) Illustration of the two spin-split electron states in the  $K/K'$  valley and possible optical transitions for zero and finite magnetic field.

with the expected diamagnetic shift of a bound particle in 2D,  $\Delta E_{\text{dia}} = e^2 \langle r^2 \rangle B_{\perp}^2 / 8m_r$ [49, 50]. The root mean square radius in the plane of the 2D material is expressed as  $r_{\text{rms}} = \sqrt{8m_r \sigma} / e$ , where  $m_r$  is the reduced mass of the particle and  $e$  the elementary charge, respectively. The observed diamagnetic shift coefficient of Q1 is roughly  $5\times$  larger than that of the neutral MoS<sub>2</sub> exciton[49, 50]. Assuming the reduced mass for the neutral exciton and Q1 are the same, ( $m_r = 0.275 m_0$ [50]), the observed diamagnetic shift yields a particle size  $r_{\text{rms}} = 3.5 \text{ nm}$ , consistent with the findings of the independent boson model discussed above. The valley Zeeman splitting, defined from the difference  $E_{\sigma^+} - E_{\sigma^-} = \mu_{\perp} B$  is shown in Fig. 2d. In contrast to other quantum emitters in 2D materials[17–20, 35, 54, 55], the Q1 emission shows little, but experimentally detectable, positive valley Zeeman splitting of  $\mu_{\perp,Q1} = +0.1 \pm 0.1 \mu_B$ . Such a vanishing Zeeman splitting has recently been observed on a quantum emission and was attributed to a quasiparticle transition between pristine conduction band and in-gap defect state[56]. However, the latter study does not provide

a full evaluation on the excitonic effects, which are crucial for magneto-spectroscopy in TMDs. In order to get a first insight into the nature of the Q1 emission line, Figure 2e shows the DFT-GW bandstructure of MoS<sub>2</sub> with a 2 % sulfur vacancy density. The pristine bandstructure of MoS<sub>2</sub> is essentially unaffected by the presence of the sulfur vacancies. However, additional electronic states lie within the bandgap (cD1, cD2), as well as in the valence band (vD) of MoS<sub>2</sub>. These states are relatively flat in k-space, which yields a high joint density of states for defect-to-defect transitions in this system (cf. density of states plot in Fig. 2f), particularly at the  $\Gamma$ -point. For a pure defect-to-defect transition at the  $\Gamma$ -point, we expect exactly zero valley Zeeman splitting due to the vanishing of the valley selectivity. In turn, the finite valley Zeeman splitting is consistent with a Q1 emission dominated by defect-to-defect transitions at the  $\Gamma$ -point and its hybridization with defect-to-band transitions at the  $K/K'$ -points, which we discuss in detail below.

Although we find  $\mu_{\perp,Q1} \approx 0$ , we measure a large degree of circular polarization (Fig. 1d) at high magnetic

fields, calculated from the integrated PL intensities of both helicities  $(I_{\sigma+} - I_{\sigma-})/(I_{\sigma+} + I_{\sigma-})$ . This  $B$ -field induced circular polarization requires spin polarized states to participate in the optical transition. The measured DCP at  $B_{\perp} = 0$  T is within the experimental uncertainty of  $\pm 10\%$  (indicated by the shaded area in Fig. 1d). The uncertainty originates from spectral jitter as well as uncompensated Faraday rotation of the linearly polarized excitation light combined with imperfectly aligned  $\lambda/4$  and linear polarizers in the detection path. The DCP as a function of applied magnetic field can be fitted using the Fermi-Dirac distribution:

$$\text{DCP}(B) = \frac{1}{\exp\left(\frac{\Delta\mu_{\text{cD1}} \cdot B + E_{\text{cD1}} - E_F}{k_B T}\right) + 1}, \quad (1)$$

with the Zeeman splitting of the occupied cD1 states in the  $K/K'$  valley  $\Delta\mu_{\text{cD1}} \cdot B = (\mu_{\text{cD1},\downarrow,K} - \mu_{\text{cD1},\uparrow,K'}) \cdot B$ , the absolute energy of the unoccupied electron state involved in the optical transition at 0 T,  $E_{\text{cD1}}$ , the Fermi energy  $E_F$ , the Boltzmann constant  $k_B$ , and the bath temperature  $T$ . With increasing  $B_{\perp}$  the DCP clearly rises to 50% at 22.5 T, reaching 84% at the highest available magnetic fields of 27 T. Taking the systematic error of our polarization alignment into account, the fit of the DCP with Eq. 1 yields  $E_{\text{cD1}} - E_F = 3.4 \pm 0.7$  meV and  $\Delta\mu_{\text{cD1}} = -2.6 \pm 0.5 \mu_B$ . This observation is in very good agreement with the theoretically predicted  $\Delta\mu_{\text{cD1}} = -2.21 \mu_B$  and clearly suggests that cD1 is a state contributing to the Q1 emission. As a consequence, an applied magnetic field lifts the spin degeneracy of Q1. Additionally, the deduced parameters suggest that  $E_F$  is roughly 3 meV below the unoccupied electron state cD1 at  $B_{\perp} = 0$ . This is consistent with the very small electron density in our sample. The polarization of the emitted light at higher magnetic fields originates from the close proximity of the cD1 states to the Fermi edge. Figure 2g illustrates the bandstructure at  $K/K'$  and  $\Gamma$  for zero and finite  $B_{\perp}$ . With increasing magnetic fields, the spin-up state of cD1 in the  $K$  valley is pushed away from the Fermi edge, which decreases the possibility for it to be occupied with an electron from the Fermi edge. This increases the part of  $\sigma^+$  polarized light emitted at the  $K$ -point and eventually polarizes the overall emission. Conversely, at the  $K'$ -point, the spin-down defect state is pushed towards the Fermi edge. Therefore, the intensity of  $\sigma^-$  polarized light subsequently diminishes. Strong reduction of the Q1 emission as a function of Fermi energy has been recently observed by gate dependent experiments at zero magnetic field[27]. Our observed energetic alignment between the defect state and the Fermi edge  $E_D - E_F = 3.4 \pm 0.7$  meV are consistent with those experiments. Therefore, from the combined experimental observations of small valley Zeeman splitting and strongly  $B_{\perp}$ -dependent DCP, we identify Q1 as an excitonic emission of a neutral sulfur vacancy in MoS<sub>2</sub> between hybridized defect-to-defect and defect-to-band transitions

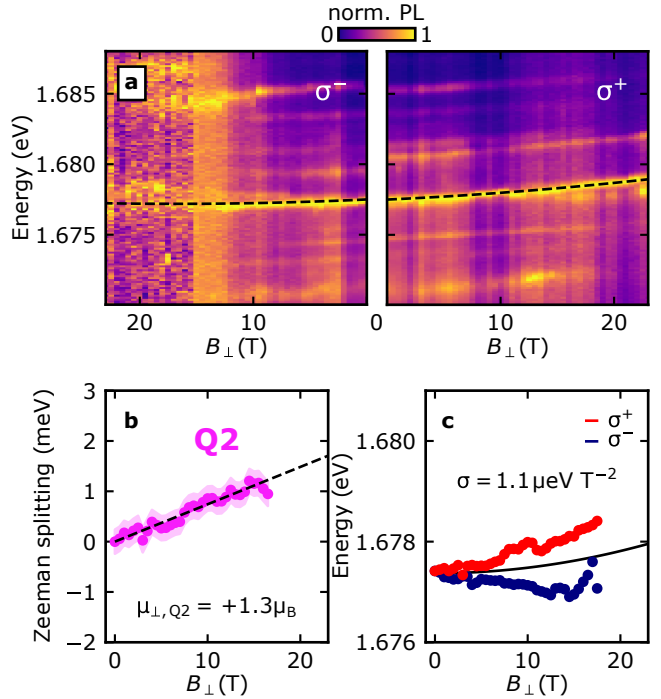


**Figure 3 | Out-of-plane magnetic field  $B_{\perp}$  dependent photoluminescence of defect luminescence Q2** a) PL of Q2 versus  $B_{\perp}$  for  $\sigma^-$  (left panel) and  $\sigma^+$  polarized detection (right panel). b) The Zeeman splitting of Q2 shows a Zeeman splitting of  $\mu_{\perp} = +1.3 \pm 0.1 \mu_B$ . c) Position of the ZPL of Q2 versus the applied magnetic field ( $B_{\perp}$ ), showing a diamagnetic shift of  $\sigma = 1.1 \pm 0.2 \mu\text{eV T}^{-2}$ .

and relate the observed DCP to a combination of magnetic field induced Zeeman shifts and occupation effects.

The  $B_{\perp}$ -dependence of the LPM emission mirrors that of Q1, as expected, with a diamagnetic shift of  $\sigma = 1.00 \pm 0.04 \mu\text{eV T}^{-2}$ , a negligible  $\mu_{\perp}$  and the same DCP trend as Q1 (see Supplementary Information Fig. S3). The similar magnetic field dependence of Q1 and LPM firmly supports the claim that the LPM emission is a replica of the same optical transition as Q1 with the additional emission of a phonon related to a local mode of the defect center[45, 57].

We now turn to the magneto-spectroscopy of the emission line Q2. Figure 3a shows polarization resolved spectra of the quantum emission Q2 as a function of magnetic field. We focus on the dominant peak at 1.677 eV, and note that fainter peaks observed at this particular spot on the sample shift equally with  $B_{\perp}$  (see Supplemental Information Section II for magneto-spectroscopy of more locations). Unlike Q1, we observe a sizeable valley Zeeman shift. This observation necessitates the lifting of valley degeneracy with increasing magnetic field and points towards optical transitions at the  $K/K'$ -points. The extracted valley Zeeman splitting is depicted in Figure 3b and yields a positive magnetic moment  $\mu_{\text{perp}} = +1.3 \pm 0.1 \mu_B$ , a sign that is opposite to the neutral ex-

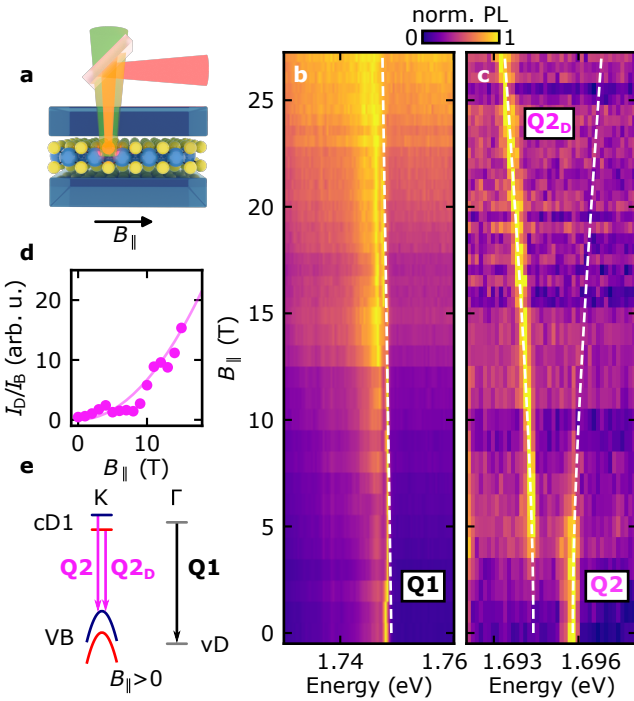


**Figure 4 | In-plane magnetic field  $B_{\parallel}$  measurements on the photoluminescence of defect luminescence Q1 and Q2.** a) Sketch of the in-plane magnetic field  $B_{\parallel}$  configuration (Voigt Geometry). No polarization optics were used in the detection path. b) Emission of Q1 remains bright for all fields. c) The in-plane field reveals a second state  $Q2_D$  energetically below Q2. The white dashed lines are guides to the eye for the expected in-plane Zeeman shift of Q1 and the dark-bright-splitting of Q2. The dark-bright splitting  $\Delta_{DB} = 1.4 \text{ meV}$  for Q2 is calculated with Eq. 2. d) The quadratic dependence of the emission ratio between  $Q2_D$  and Q2 indicates the brightening of a dark ground state. e) Sketch of the defect levels with the possible optical transitions for Q1 and Q2 at finite  $B_{\parallel}$ .

citon of the host  $\text{MoS}_2$ . Furthermore, similar to Q1, we observe a diamagnetic shift with  $\sigma_{Q2} = 1.1 \pm 0.2 \mu\text{eV T}^{-2}$  (Fig. 3c), indicating again that this emission originates from a bound state. The magnetic field dependent DCP of Q2 (see Figure 1c) shows qualitatively the same behaviour as Q1 and can also be fit with equation 1, yielding  $\Delta\mu_{cD1} = -2.1 \pm 0.5 \mu_B$  and  $E_{cD1} - E_F = 1.4 \pm 0.7 \text{ meV}$  (note that  $E_F$  varies locally throughout our sample). Within our experimental uncertainties, this supports again that cD1 contributes to the optical transition Q2.

### C. In-plane magnetic field measurements on defects in $\text{MoS}_2$

To further investigate the details of the electronic states involved in the emission lines Q1 and Q2, we turn to magneto-spectroscopy in the Voigt configuration for which the magnetic field ( $B_{\parallel}$ ) is applied parallel to the sample plane and perpendicular to the optical beam path (see Fig. 4a and Supplementary Information Section III for data on  $Q^*$ ). In monolayer TMDs, strong spin-orbit coupling leads to out-of plane spin eigenstates particularly at the  $K/K'$  points in the Brillouin zone. In principle, an in-plane magnetic field  $B_{\parallel}$  induces a precession of the out-of-plane spins, leading to an increased mixing of the spin-eigenstates with increasing  $B_{\parallel}$ . This mixing results in a magnetic-field dependent brightening of spin-forbidden transitions at  $K/K'$  with the intensity of the dark transitions increasing relative to the bright transitions with  $B_{\parallel}^2$ [58–60]. Figure 4b shows a colormap of the PL versus  $B_{\parallel}$  for Q1. We observe a monotonous redshift of the emission line, which is accompanied with spectral jitter with increasing magnetic field. Importantly, no brightening of a lower lying emission line is observed. The dashed white line in Fig. 4b is a guide to the eye that shows a redshift of Q1 with an in-plane magnetic moment  $\mu_{\parallel} = -1 \mu_B$ .

The in-plane magneto-PL of a typical Q2 quantum emitter is shown in Figure 4c. At  $B_{\parallel} = 0 \text{ T}$ , one emission line is observed at 1.696 eV. This line diminishes with increasing  $B_{\parallel}$ , while a new peak, 1.4 meV red-shifted from the original Q2 emission line, quickly appears above 3 T. Figure 4d shows the integrated PL ratio of the two lines together with a quadratic-in- $B$  fit, consistently describing the brightening of a dark transition. The low energy peak continues to red-shift with increasing  $B_{\parallel}$ . This behavior can be described with the magnetic field induced splitting of a dark and bright emission branch[61]

$$\Delta(B_{\parallel}) = \left( \Delta_{DB} \pm \sqrt{\Delta_{DB}^2 + (\mu_{\parallel} \cdot B_{\parallel})^2} \right), \quad (2)$$

where  $\Delta_{DB}$  is the dark-bright splitting at  $B_{\parallel} = 0 \text{ T}$  and  $|\mu_{\parallel}|$  is the magnitude of the in-plane magnetic moment. The white dashed line in Figure 4c depicts Equation 2 with  $\Delta_0 = 1.4 \text{ meV}$  and  $|\mu_{\parallel}| = 1 \mu_B$ . The excellent agreement between data and fit shows the brightening of a dark transition. This observation necessitates the involvement of two spin states in Q2, while the observation of the valley Zeeman splitting shown above requires the breaking of valley degeneracy. As such, we conclude that Q2 must be a superposition of transitions involving both cD1 states and the valence band of the host  $\text{MoS}_2$  (Fig. 4e). For neutral excitons in TMDs, a redshift with increasing  $B_{\parallel}$  was explained with the average valley Zeeman shift of a bright and dark state ( $|\mu_{\perp,dark}| - |\mu_{\perp,bright}| = 2|\mu_{\parallel}|$ )[58, 59, 61]. Our observed shift is in very good agreement with the calculated difference of the bright and dark transition of Q2, which is simply given by the Zeeman splitting of the cD1 band

( $\Delta\mu_{cD1} = -2.1 \pm 0.50 \mu_B$ ), measured above. Finally, the combined magneto-spectroscopy in the Faraday and Voigt geometry unambiguously identifies Q2 as a spin conserving transition from the cD1 state to the respective MoS<sub>2</sub> valence band in the  $K/K'$  valley.

The fact that the emission line Q1 is energetically higher than Q2, while the diamagnetic shift, and therefore the binding energy of Q1 and Q2 are essentially the same, requires the defect band  $vD$  to be located below the valence band edge of MoS<sub>2</sub>, as sketched in Fig. 4e[46–48].

#### D. First-principles calculations on monolayer MoS<sub>2</sub> with embedded sulfur vacancies

To deepen the insight into the nature of Q1 and Q2, we theoretically investigate exciton transitions in monolayer MoS<sub>2</sub> with embedded sulfur vacancies using ab initio calculations. Details about the calculation can be found in the Supplementary Information section IV as well as the Methods section of[46, 47, 62]. In brief, we use many-body perturbation theory within the GW-Bethe-Salpeter approximation with explicit spin-orbit coupling and spinor wavefunctions and compute the many-body Zeeman splitting following[63]. Figure 5a shows the mean calculated Zeeman splitting for an excitonic absorption as a function of excitation energy. Line colors represent the calculated absorption strength for  $\sigma^+$  polarized light. The mean Zeeman splitting at each energy is calculated by averaging the Zeeman splitting of all discrete excitons composing the overall optical absorption in a narrow energy band. The transitions are broadened with a Gaussian and weighted by the oscillator strength of the respective excitons. It has previously been shown[46, 47, 62], that the energetically lowest interband transitions are mainly composed of pristine MoS<sub>2</sub> valence band to defect band transitions. The strongly varying average exciton Zeeman splitting is testament of approximately conserved valley selectivity in this energy range, which sensitively depends on the distinct electron-hole transitions in a specific energy interval. We observe strong variations of the exciton Zeeman splitting in the energy range below  $\approx 1.70$  eV, originating from the hybridization of the BSE excitations, which mix electron-hole transitions from defect and non-defect bands. Specifically in the range of  $\approx 1.64$  eV –  $1.68$  eV we observe a significant increase of the Zeeman splitting, consistent with our observation for the Q2 emission. This is a result of allowed transitions to in-gap defect states of both spin components (see Fig. 1c) In Fig. 5b,c and d we show the normalized contributions of electron-hole transitions composing the excitons in this energy range (magenta shaded area in 5a) at three representative points in the Brillouin zone ( $K$ ,  $\Gamma$ , and  $K'$ ). The height of each bar corresponds to the relative contribution of transitions from an occupied state (x-axis) to an unoccupied state (y-axis) upon excitation with  $\sigma^+$  polarized light. At the  $K/K'$  points,

we find strong contributions for electron-hole transitions between the pristine-like MoS<sub>2</sub> valence band and both spin states of cD1. As a result, in the region of positive average Zeeman splitting, the contribution is highest for transitions from the upper MoS<sub>2</sub> valence band to the defect state cD1, as contributions at the  $\Gamma$ -point are comparatively reduced. For Q1, the energy range between  $\approx 1.74$  eV –  $1.79$  eV is selected. In this energy range, the absorption strength dominates, which is consistent with the dominating PL of Q1 as compared to the other defect emission bands. Furthermore, a slightly positive exciton Zeeman splitting is calculated, which again is consistent with our observations in Figure 2d. Figure 5e,f and g shows the contributions of electron-hole transitions composing the exciton in the corresponding energy range. At the  $K/K'$ -points, only band-to-defect transitions are contributing, whereas at the  $\Gamma$ -point defect-to-defect transitions are dominating. Moreover, at the  $K/K'$ -points, we find contributions from the lower valence band to defect band cD2 in absorption. This transition is an analogue of the neutral B exciton in MoS<sub>2</sub>, and is hence less pronounced in PL measurements. The calculations suggest that the Q2 emission has only contributions at the  $K/K'$ -points with band-to-defect transitions. The Q1 emission has additional contributions of defect-to-defect character at the  $\Gamma$ -point. The hybridization of Q1 with the energetically lower lying Q2 emission can be deduced from the band-to-defect contributions at the  $K/K'$ -points.

### III. DISCUSSION

In order to characterize the defect luminescence, Q1, Q2 and Q\* of He-ion irradiated monolayer MoS<sub>2</sub> towards spin defect properties, we combine our experimental observations with theoretical insight. He ions induce sulfur vacancies, which induce flat defect bands throughout the pristine bandstructure of monolayer MoS<sub>2</sub>. As a result, a high joint DOS for defect-to-defect transitions is created. At the  $K/K'$ -points however, the defect  $vD$  lies below the valence band maximum of MoS<sub>2</sub>, such that defect-to-band transitions are more likely. In high field magneto-spectroscopy, we observe a diamagnetic shift of the defect luminescence Q1 and Q2, which is consistent with a bound particle of  $\sim 3.5$  nm. This localized character will result in optical transitions covering a significant momentum-space. Thus, the GW-Bethe-Salpeter equation is useful for gaining deeper understanding into the defect-induced transitions. Here we find that the nature of Q1 and Q2 can be viewed as mixed states of defect-to-defect and defect-to-band transitions. The level of this admixture will determine the magnetic moment and valley selectivity of these hybridized transitions [46, 62]. We find a dominant contribution of band-to-defect transitions at the  $K/K'$ -points for the energy interval of Q2, whereas Q1 additionally acquires sizeable defect-to-defect character from the  $\Gamma$ -point. These contributions at the  $\Gamma$ -point induce a breaking of the valley

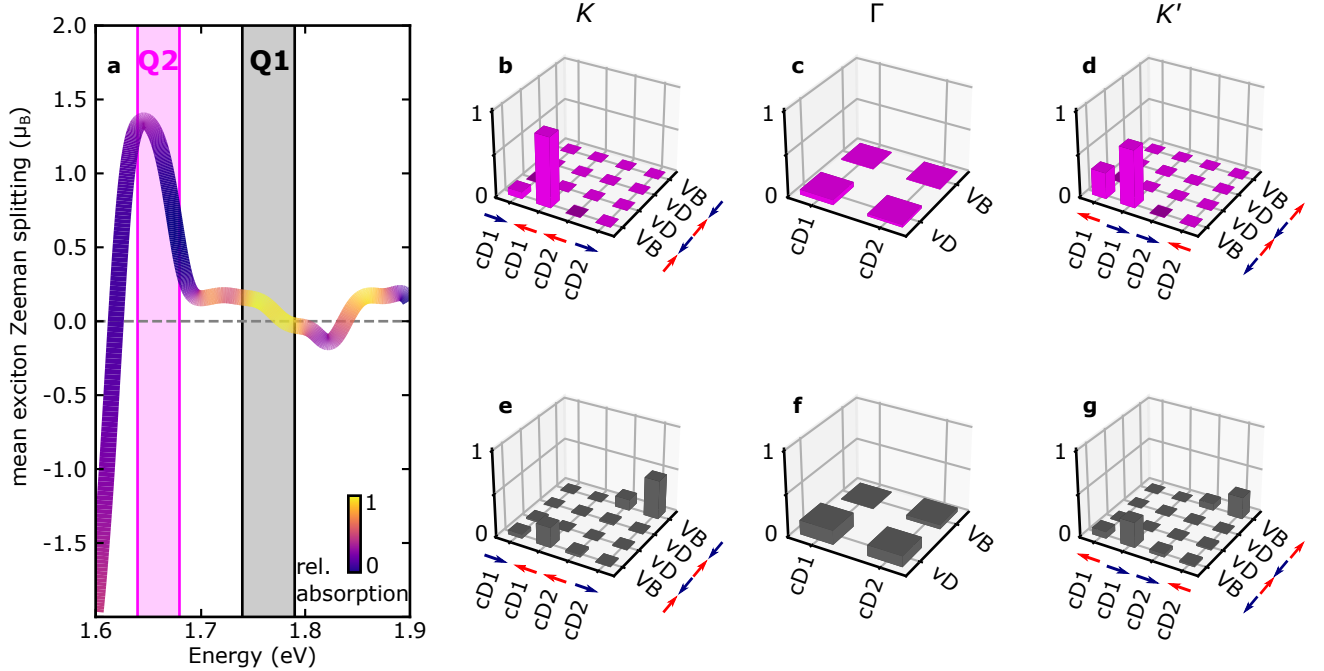


**Figure 5 | GW-BSE results for optical absorption, exciton Zeeman splitting, and transition contributions.** a) Mean exciton Zeeman splitting as a function of excitation energy. The colorcode on the line represents the absorption strength at each energy. b,c,d) Electron-hole transitions contributing to excitons in the energy range associated with Q2, namely in the magenta shaded area in (a). The electron bands ( $cD_1$  and  $cD_2$ ), as well as the hole bands ( $vD$  and  $VB$ ) are illustrated in energetic order under the consideration of the lifted spin degeneracy at the  $K/K'$ -points. e,f,g) Electron-hole transitions contributing to excitons in the energy range associated with Q1, namely in the grey shaded area in (a). The transitions are shown for three selective k-points,  $K$  (b,e),  $\Gamma$  (c,f), and  $K'$  (d,g).

selectivity, reflected in the small valley Zeeman splitting of this transition. For both Q1 and Q2, however, we find a magnetic-field dependent DCP, which necessitates spin conserving optical transitions. The distinct behavior of the DCP is explained by the defect-to-band transitions at the  $K/K'$ -points contributing to Q1 and Q2. The in-plane magneto-spectroscopy reveals a spin-forbidden dark ground state for Q2, which unambiguously proofs the lifted spin degeneracy of the defect bands at the  $K/K'$ -points even at zero magnetic field. In contrast, the absence of a dark state for Q1 can be explained by the significant portion of transitions happening at the  $\Gamma$ -point, where the defect bands are spin degenerate due to Kramers' theorem.

In conclusion, the combination of in-plane and out-of-plane magneto-spectroscopy unambiguously identifies the Q1 emission as a defect-to-defect transition with admixture of Q2, which is dominated by transitions from in-gap defect states to the pristine valence band of MoS<sub>2</sub>. This outcome suggests tailored modification of the defect luminescence through either charging or chemical modification (Q\*, see Supplemental Information Section II and III). We show that the defect states at  $K/K'$  are split at zero magnetic field, a property that characterizes the sulfur vacancy in MoS<sub>2</sub> as a spin defect with desirable features for quantum technological applications.

## IV. METHODS

### A. Sample preparation

MoS<sub>2</sub> bulk crystals were purchased from HQGraphene, and the hBN crystals were provided by Takashi Taniguchi and Kenji Watanabe from NIMS, Japan. Monolayers of MoS<sub>2</sub> and few-layer hBN were obtained by mechanical cleavage of bulk crystals. The thin crystals were stacked with the viscoelastic transfer method onto a Si substrate with 285 nm of thermal SiO<sub>2</sub>. After the assembly of the desired heterostructure, namely the MoS<sub>2</sub> encapsulated in hBN, the helium ion microscope (HIM) Orion NanoFab from Zeiss was used to precisely irradiate the sample with He-ions at 30 kV in an array pattern with a pitch of 2  $\mu\text{m}$ . The dose was chosen to get a high yield of single sharp emitter lines for Q1. For the photoluminescence measurements in Figure 1b an excitation wavelength of 639 nm and a power of 550 nW at a bath temperature of 1.7 K was used. The photoluminescence signal was guided on a nitrogen cooled CCD via a 300 grooves/mm dispersive grating. A long pass filter was used to extinguish the directly reflected excitation laser emission.

## B. Magneto-spectroscopy

The photoluminescence measurements were performed in a cryostat cooled to 4.2 K surrounded by a resistive magnet. For excitation, a laser diode with an emission wavelength of 515 nm was used. For the measurements in Faraday configuration (B-field perpendicular to the sample plane and parallel to the optical beam path), the linearly polarized excitation was focused on the sample with an objective with NA = 0.81. The reflected light was collected with the same objective and guided through a  $\lambda/4$ -plate followed by a linear polarizer to select the  $\sigma^+$  ( $\sigma^-$ ) polarized light in the detection. A long pass filter was used to extinguish the directly reflected excitation laser emission. The collected light was analyzed in a spectrometer equipped with a liquid nitrogen cooled CCD and a 600 grooves/mm dispersive grating. For measurements in Voigt configuration (B-field parallel to the sample plane and perpendicular to the optical beam path) the sample was mounted vertically and the detection was unpolarized. A mirror tilted by 45° was used to guide incident light perpendicular to the sample plane. A large working distance objective with NA = 0.35 was used to focus the excitation laser via the tilted mirror onto the sample and

collect the reflected light.

## C. Ab-initio calculations

State-of-the-art ab initio ground-state and excited-state calculations were carried out in a  $5 \times 5 \times 1$  supercell of monolayer MoS<sub>2</sub> composed of 74 atoms and a single sulphur vacancy. Ground state DFT calculations were performed using the Quantum Espresso package[64, 65] for assessing the atomic structure, spinor wavefunctions and single-particle magnetization, with an energy cutoff of 75 Ry. These properties were used as a starting point for a GW[66] calculation of the quasi-particle energies, including spin-orbit coupling within the BerkeleyGW[67] software, with summation over 3998 bands on a  $3 \times 3 \times 1$  k-grid and an energy cutoff of 25 Ry for the dielectric matrix. Electron-hole coupling and exciton energies were calculated using BerkeleyGW by solving the Bethe-Salpeter equation (BSE)[68, 69] by interpolating the GW results to a k-grid of  $6 \times 6 \times 1$  with a dielectric matrix which was calculated with a 5 Ry cutoff and summation over 1798 bands. Quasi-particle magnetization corrections and many-body excitonic Zeeman splitting were evaluated from the GW-BSE results following recently derived methods[63, 70]. More details are presented in the Supplementary Information Section IV.

- 
- [1] A. Reserbat-Plantey, I. Epstein, I. Torre, A. T. Costa, P. A. D. Gonçalves, N. A. Mortensen, M. Polini, J. C. W. Song, N. M. R. Peres, and F. H. L. Koppens, Quantum Nanophotonics in Two-Dimensional Materials, *ACS Photonics* **8**, 85 (2021).
- [2] A. Gottscholl, M. Diez, V. Soltamov, C. Kasper, D. Krause, A. Sperlich, M. Kianinia, C. Bradac, I. Aharonovich, and V. Dyakonov, Spin defects in hBN as promising temperature, pressure and magnetic field quantum sensors., *Nature communications* **12**, 4480 (2021).
- [3] M. Turunen, M. Brotons-Gisbert, Y. Dai, Y. Wang, E. Scerri, C. Bonato, K. D. Jöns, Z. Sun, and B. D. Gerardot, Quantum photonics with layered 2D materials, *Nature Reviews Physics* , 1 (2022).
- [4] A. Gruber, A. Dräbenstedt, C. Tietz, L. Fleury, J. Wrachtrup, and C. von Borczyskowski, Scanning confocal optical microscopy and magnetic resonance on single defect centers, *Science* **276**, 2012 (1997).
- [5] M. W. Doherty, N. B. Manson, P. Delaney, F. Jelezko, J. Wrachtrup, and L. C. Hollenberg, The nitrogen-vacancy colour centre in diamond, *Physics Reports* **528**, 1 (2013).
- [6] V. Dobrovitski, G. Fuchs, A. Falk, C. Santori, and D. Awschalom, Quantum Control over Single Spins in Diamond, *Annual Review of Condensed Matter Physics* **4**, 23 (2013).
- [7] F. Casola, T. van der Sar, and A. Yacoby, Probing condensed matter physics with magnetometry based on nitrogen-vacancy centres in diamond, *Nature Reviews Materials* **3**, 17088 (2018).
- [8] C. Bradac, W. Gao, J. Forneris, M. E. Trusheim, and I. Aharonovich, Quantum nanophotonics with group IV defects in diamond, *Nature Communications* **10**, 5625 (2019), arXiv:1906.10992.
- [9] S. Hernández-Gómez and N. Fabbri, Quantum Control for Nanoscale Spectroscopy With Diamond Nitrogen-Vacancy Centers: A Short Review, *Frontiers in Physics* **8**, 652 (2021).
- [10] A. Dräbenstedt, L. Fleury, C. Tietz, F. Jelezko, S. Kilin, A. Nizovtzev, and J. Wrachtrup, Low-temperature microscopy and spectroscopy on single defect centers in diamond, *Physical Review B* **60**, 11503 (1999).
- [11] R. Brouri, A. Beveratos, J.-P. Poizat, and P. Grangier, Photon antibunching in the fluorescence of individual color centers in diamond, *Optics Letters* **25**, 1294 (2000).
- [12] C. Kurtsiefer, S. Mayer, P. Zarda, and H. Weinfurter, Stable Solid-State Source of Single Photons, *Physical Review Letters* **85**, 290 (2000).
- [13] K. Ohno, F. Joseph Heremans, L. C. Bassett, B. A. Myers, D. M. Toyli, A. C. Bleszynski Jayich, C. J. Palmstrøm, and D. D. Awschalom, Engineering shallow spins in diamond with nitrogen delta-doping, *Applied Physics Letters* **101**, 082413 (2012).
- [14] J. Martin, R. Wannemacher, J. Teichert, L. Bischoff, and B. Köhler, Generation and detection of fluorescent color centers in diamond with submicron resolution, *Applied Physics Letters* **75**, 3096 (1999).
- [15] M. Lesik, P. Spinicelli, S. Pezzagna, P. Happel, V. Jacques, O. Salord, B. Rasser, A. Delobbe, P. Su

- draud, A. Tallaire, J. Meijer, and J.-F. Roch, Maskless and targeted creation of arrays of colour centres in diamond using focused ion beam technology, *physica status solidi (a)* **210**, 2055 (2013).
- [16] S. Pezzagna, D. Wildanger, P. Mazarov, A. D. Wieck, Y. Sarov, I. Rangelow, B. Naydenov, F. Jelezko, S. W. Hell, and J. Meijer, Nanoscale Engineering and Optical Addressing of Single Spins in Diamond, *Small* **6**, 2117 (2010).
- [17] Y.-M. He, G. Clark, J. R. Schaibley, Y. He, M.-C. Chen, Y.-J. Wei, X. Ding, Q. Zhang, W. Yao, X. Xu, C.-Y. Lu, and J.-W. Pan, Single quantum emitters in monolayer semiconductors, *Nature Nanotechnology* **10**, 497 (2015).
- [18] C. Chakraborty, L. Kinnischtzke, K. M. Goodfellow, R. Beams, and A. N. Vamivakas, Voltage-controlled quantum light from an atomically thin semiconductor, *Nature Nanotechnology* **10**, 507 (2015).
- [19] A. Srivastava, M. Sidler, A. V. Allain, D. S. Lembke, A. Kis, and A. Imamoğlu, Optically active quantum dots in monolayer  $\text{WeS}_2$ , *Nature Nanotechnology* **10**, 491 (2015).
- [20] M. Koperski, K. Nogajewski, A. Arora, V. Cherkez, P. Mallet, J.-Y. Veuillet, J. Marcus, P. Kossacki, and M. Potemski, Single photon emitters in exfoliated  $\text{WSe}_2$  structures, *Nature Nanotechnology* **10**, 503 (2015).
- [21] P. Tonndorf, R. Schmidt, R. Schneider, J. Kern, M. Buscema, G. A. Steele, A. Castellanos-Gomez, H. S. J. van der Zant, S. Michaelis de Vasconcellos, and R. Bratschitsch, Single-photon emission from localized excitons in an atomically thin semiconductor, *Optica* **2**, 347 (2015).
- [22] T. T. Tran, K. Bray, M. J. Ford, M. Toth, and I. Aharonovich, Quantum emission from hexagonal boron nitride monolayers, *Nature Nanotechnology* **11**, 37 (2016).
- [23] K. F. Mak, C. Lee, J. Hone, J. Shan, and T. F. Heinz, Atomically thin  $\text{MoS}_2$ : A new direct-gap semiconductor, *Physical Review Letters* **105**, 136805 (2010).
- [24] D. Xiao, G.-B. Liu, W. Feng, X. Xu, and W. Yao, Coupled Spin and Valley Physics in Monolayers of  $\text{MoS}_2$  and Other Group-VI Dichalcogenides, *Physical Review Letters* **108**, 196802 (2012).
- [25] Z. Lin, B. R. Carvalho, E. Kahn, R. Lv, R. Rao, H. Terrones, M. A. Pimenta, and M. Terrones, Defect engineering of two-dimensional transition metal dichalcogenides, *2D Materials* **3**, 022002 (2016).
- [26] A. Mukherjee, C. Chakraborty, L. Qiu, and A. N. Vamivakas, Electric field tuning of strain-induced quantum emitters in  $\text{WSe}_2$ , *AIP Advances* **10**, 75310 (2020).
- [27] A. Hötger, J. Klein, K. Barthelmi, L. Sigl, F. Sigger, W. Männer, S. Gyger, M. Florian, M. Lorke, F. Jahnke, T. Taniguchi, K. Watanabe, K. D. Jöns, U. Wurstbauer, C. Kastl, K. Müller, J. J. Finley, and A. W. Holleitner, Gate-Switchable Arrays of Quantum Light Emitters in Contacted Monolayer  $\text{MoS}_2$  van der Waals Heterostructures, *Nano Letters* **21**, 1040 (2021).
- [28] C. Palacios-Berraquero, M. Barbone, D. M. Kara, X. Chen, I. Goykhman, D. Yoon, A. K. Ott, J. Beitterer, K. Watanabe, T. Taniguchi, A. C. Ferrari, and M. Atatüre, Atomically thin quantum light-emitting diodes, *Nature Communications* **7**, 12978 (2016).
- [29] S. Schwarz, A. Kozikov, F. Withers, J. K. Maguire, A. P. Foster, S. Dufferwiel, L. Hague, M. N. Makhonin, L. R. Wilson, A. K. Geim, K. S. Novoselov, and A. I. Taratkovskii, Electrically pumped single-defect light emitters in  $\text{WSe}_2$ , *2D Materials* **3**, 025038 (2016).
- [30] G. Clark, J. R. Schaibley, J. Ross, T. Taniguchi, K. Watanabe, J. R. Hendrickson, S. Mou, W. Yao, and X. Xu, Single Defect Light-Emitting Diode in a van der Waals Heterostructure, *Nano Letters* **16**, 3944 (2016).
- [31] S. Kumar, A. Kaczmarczyk, and B. D. Gerardot, Strain-Induced Spatial and Spectral Isolation of Quantum Emitters in Mono- and Bilayer  $\text{WSe}_2$ , *Nano Letters* **15**, 7567 (2015), arXiv:1509.01085.
- [32] J. Kern, I. Niehues, P. Tonndorf, R. Schmidt, D. Wigger, R. Schneider, T. Stiehm, S. Michaelis de Vasconcellos, D. E. Reiter, T. Kuhn, and R. Bratschitsch, Nanoscale Positioning of Single-Photon Emitters in Atomically Thin  $\text{WSe}_2$ , *Advanced Materials* **28**, 7101 (2016).
- [33] A. Branny, S. Kumar, R. Proux, and B. D. Gerardot, Deterministic strain-induced arrays of quantum emitters in a two-dimensional semiconductor, *Nature Communications* **8**, 15053 (2017), arXiv:1610.01406.
- [34] C. Palacios-Berraquero, D. M. Kara, A. R.-P. Montblanch, M. Barbone, P. Latawiec, D. Yoon, A. K. Ott, M. Loncar, A. C. Ferrari, and M. Atatüre, Large-scale quantum-emitter arrays in atomically thin semiconductors, *Nature Communications* **8**, 15093 (2017).
- [35] A. Branny, G. Wang, S. Kumar, C. Robert, B. Lassagne, X. Marie, B. D. Gerardot, and B. Urbaszek, Discrete quantum dot like emitters in monolayer  $\text{MoSe}_2$ : Spatial mapping, magneto-optics, and charge tuning, *Applied Physics Letters* **108**, 142101 (2016), arXiv:1602.07947.
- [36] N. V. Proscia, Z. Shotan, H. Jayakumar, P. Reddy, C. Cohen, M. Dollar, A. Alkauskas, M. Doherty, C. A. Meriles, and V. M. Menon, Near-deterministic activation of room-temperature quantum emitters in hexagonal boron nitride, *Optica* **5**, 1128 (2018), arXiv:1712.01352.
- [37] K. Parto, S. I. Azzam, K. Banerjee, and G. Moody, Defect and strain engineering of monolayer  $\text{WSe}_2$  enables site-controlled single-photon emission up to 150 K, *Nature Communications* **12**, 3585 (2021).
- [38] H.-P. Komsa, J. Kotakoski, S. Kurasch, O. Lehtinen, U. Kaiser, and A. V. Krasheninnikov, Two-Dimensional Transition Metal Dichalcogenides under Electron Irradiation: Defect Production and Doping, *Physical Review Letters* **109**, 035503 (2012).
- [39] G. Moody, K. Tran, X. Lu, T. Autry, J. M. Fraser, R. P. Mirin, L. Yang, X. Li, and K. L. Silverman, Microsecond Valley Lifetime of Defect-Bound Excitons in Monolayer  $\text{WSe}_2$ , *Physical Review Letters* **121**, 057403 (2018).
- [40] J. Klein, M. Lorke, M. Florian, F. Sigger, L. Sigl, S. Rey, J. Wierzbowski, J. Cerne, K. Müller, E. Mitterreiter, P. Zimmermann, T. Taniguchi, K. Watanabe, U. Wurstbauer, M. Kaniber, M. Knap, R. Schmidt, J. J. Finley, and A. W. Holleitner, Site-selectively generated photon emitters in monolayer  $\text{MoS}_2$  via local helium ion irradiation, *Nature Communications* **10**, 2755 (2019).
- [41] C. Fournier, A. Plaud, S. Roux, A. Pierret, M. Rosticher, K. Watanabe, T. Taniguchi, S. Buil, X. Quélin, J. Barjon, J.-P. Hermier, and A. Delteil, Position-controlled quantum emitters with reproducible emission wavelength in hexagonal boron nitride, *Nature Communications* **2021** 12:1 **12**, 1 (2021).
- [42] S. Kretschmer, M. Maslov, S. Ghaderzadeh, M. Ghorbani-Asl, G. Hlawacek, and A. V. Krasheninnikov, Supported Two-Dimensional Materials under Ion Irradiation: The Substrate Governs Defect Production, *ACS Applied Materials and Interfaces* **10**, 30827 (2018).

- [43] E. Mitterreiter, B. Schuler, K. A. Cochrane, U. Wurstbauer, A. Weber-Bargioni, C. Kastl, and A. W. Holleitner, Atomistic Positioning of Defects in Helium Ion Treated Single-Layer MoS<sub>2</sub>, *Nano Letters* **20**, 4437 (2020).
- [44] K. Barthelmi, J. Klein, A. Hötger, L. Sigl, F. Sigger, E. Mitterreiter, S. Rey, S. Gyger, M. Lorke, M. Florian, F. Jahnke, T. Taniguchi, K. Watanabe, V. Zwiller, K. D. Jöns, U. Wurstbauer, C. Kastl, A. Weber-Bargioni, J. J. Finley, K. Müller, and A. W. Holleitner, Atomistic defects as single-photon emitters in atomically thin MoS<sub>2</sub>, *Applied Physics Letters* **117**, 070501 (2020).
- [45] J. Klein, L. Sigl, S. Gyger, K. Barthelmi, M. Florian, S. Rey, T. Taniguchi, K. Watanabe, F. Jahnke, C. Kastl, V. Zwiller, K. D. Jöns, K. Müller, U. Wurstbauer, J. J. Finley, and A. W. Holleitner, Engineering the Luminescence and Generation of Individual Defect Emitters in Atomically Thin MoS<sub>2</sub>, *ACS Photonics* **8**, 669 (2021).
- [46] S. Refaelly-Abramson, D. Y. Qiu, S. G. Louie, and J. B. Neaton, Defect-Induced Modification of Low-Lying Excitons and Valley Selectivity in Monolayer Transition Metal Dichalcogenides, *Physical Review Letters* **121**, 167402 (2018).
- [47] E. Mitterreiter, B. Schuler, A. Micevic, D. Hernangómez-Pérez, K. Barthelmi, K. A. Cochrane, J. Kiemle, F. Sigger, J. Klein, E. Wong, E. S. Barnard, K. Watanabe, T. Taniguchi, M. Lorke, F. Jahnke, J. J. Finley, A. M. Schwartzberg, D. Y. Qiu, S. Refaelly-Abramson, A. W. Holleitner, A. Weber-Bargioni, and C. Kastl, The role of chalcogen vacancies for atomic defect emission in MoS<sub>2</sub>, *Nature Communications* **12**, 3822 (2021).
- [48] S. Gupta, J. H. Yang, and B. I. Yakobson, Two-Level Quantum Systems in Two-Dimensional Materials for Single Photon Emission, *Nano Letters* **19**, 408 (2019).
- [49] A. V. Stier, K. M. McCreary, B. T. Jonker, J. Kono, and S. A. Crooker, Exciton diamagnetic shifts and valley Zeeman effects in monolayer WS<sub>2</sub> and MoS<sub>2</sub> to 65 Tesla, *Nature Communications* **7**, 1 (2016), arXiv:1510.07022.
- [50] M. Goryca, J. Li, A. V. Stier, T. Taniguchi, K. Watanabe, E. Courtade, S. Shree, C. Robert, B. Urbaszek, X. Marie, and S. A. Crooker, Revealing exciton masses and dielectric properties of monolayer semiconductors with high magnetic fields, *Nature Communications* **10**, 1 (2019), arXiv:1904.03238.
- [51] Z. Li, T. Wang, S. Miao, Z. Lian, and S. F. Shi, Fine structures of valley-polarized excitonic states in monolayer transitional metal dichalcogenides, *Nanophotonics* **9**, 1811 (2020).
- [52] J. Klein, A. Hötger, M. Florian, A. Steinhoff, A. Delhomme, T. Taniguchi, K. Watanabe, F. Jahnke, A. W. Holleitner, M. Potemski, C. Faugeras, J. J. Finley, and A. V. Stier, Controlling exciton many-body states by the electric-field effect in monolayer MoS<sub>2</sub>, *Physical Review Research* **3**, L022009 (2021).
- [53] L. Yu, M. Deng, J. L. Zhang, S. Borghardt, B. Kardynal, J. Vučković, and T. F. Heinz, Site-Controlled Quantum Emitters in Monolayer MoSe<sub>2</sub>, *Nano Letters* **21**, 2376 (2021).
- [54] M. Brotons-Gisbert, A. Branny, S. Kumar, R. Picard, R. Proux, M. Gray, K. S. Burch, K. Watanabe, T. Taniguchi, and B. D. Gerardot, Coulomb blockade in an atomically thin quantum dot coupled to a tunable Fermi reservoir, *Nature Nanotechnology* **14**, 442 (2019).
- [55] X. Lu, X. Chen, S. Dubey, Q. Yao, W. Li, X. Wang, Q. Xiong, and A. Srivastava, Optical initialization of a single spin-valley in charged WSe<sub>2</sub> quantum dots, *Nature Nanotechnology* **14**, 426 (2019).
- [56] J. Dang, S. Sun, X. Xie, Y. Yu, K. Peng, C. Qian, S. Wu, F. Song, J. Yang, S. Xiao, L. Yang, Y. Wang, M. A. Rafiq, C. Wang, and X. Xu, Identifying defect-related quantum emitters in monolayer WSe<sub>2</sub>, *npj 2D Materials and Applications* **4**, 1 (2020).
- [57] D. Wigger, R. Schmidt, O. D. Pozo-Zamudio, J. A. Preuß, P. Tonndorf, R. Schneider, P. Steeger, J. Kern, Y. Khodaei, J. Sperling, S. M. de Vasconcellos, R. Bratschitsch, and T. Kuhn, Phonon-assisted emission and absorption of individual color centers in hexagonal boron nitride, *2D Materials* **6**, 035006 (2019).
- [58] M. R. Molas, C. Faugeras, A. O. Slobodenik, K. Nogajewski, M. Bartos, D. M. Basko, and M. Potemski, Brightening of dark excitons in monolayers of semiconducting transition metal dichalcogenides, *2D Materials* **4**, 021003 (2017), arXiv:1612.02867.
- [59] C. Robert, B. Han, P. Kapuscinski, A. Delhomme, C. Faugeras, T. Amand, M. R. Molas, M. Bartos, K. Watanabe, T. Taniguchi, B. Urbaszek, M. Potemski, and X. Marie, Measurement of the spin-forbidden dark excitons in MoS<sub>2</sub> and MoSe<sub>2</sub> monolayers, *Nature Communications* **11**, 1 (2020).
- [60] P. Kapuściński, A. Delhomme, D. Vaclavkova, A. O. Slobodenik, M. Grzeszczyk, M. Bartos, K. Watanabe, T. Taniguchi, C. Faugeras, and M. Potemski, Rydberg series of dark excitons and the conduction band spin-orbit splitting in monolayer WSe<sub>2</sub>, *Communications Physics* **4**, 186 (2021).
- [61] Z. Lu, D. Rhodes, Z. Li, D. van Tuan, Y. Jiang, J. Ludwig, Z. Jiang, Z. Lian, S. F. Shi, J. Hone, H. Dery, and D. Smirnov, Magnetic field mixing and splitting of bright and dark excitons in monolayer MoSe<sub>2</sub>, *2D Materials* **7**, 015017 (2020).
- [62] T. Amit, D. Hernangómez-Pérez, G. Cohen, D. Y. Qiu, and S. Refaelly-Abramson, Tunable magneto-optical properties in MoS<sub>2</sub> via defect-induced exciton transitions, arXiv 2203.14125 (2022), arXiv:2203.14125.
- [63] T. Deilmann, P. Krüger, and M. Rohlfing, Ab Initio Studies of Exciton g Factors: Monolayer Transition Metal Dichalcogenides in Magnetic Fields, *Physical Review Letters* **124**, 226402 (2020), arXiv:2003.00235.
- [64] P. Giannozzi, S. Baroni, N. Bonini, M. Calandra, R. Car, C. Cavazzoni, D. Ceresoli, G. L. Chiarotti, M. Cococcioni, I. Dabo, A. Dal Corso, S. de Gironcoli, S. Fabris, G. Fratesi, R. Gebauer, U. Gerstmann, C. Gougauss, A. Kokalj, M. Lazzeri, L. Martin-Samos, N. Marzari, F. Mauri, R. Mazzarello, S. Paolini, A. Pasquarello, L. Paulatto, C. Sbraccia, S. Scandolo, G. Scaluzero, A. P. Seitsonen, A. Smogunov, P. Umari, and R. M. Wentzcovitch, QUANTUM ESPRESSO: a modular and open-source software project for quantum simulations of materials., *Journal of physics. Condensed matter : an Institute of Physics journal* **21**, 395502 (2009).
- [65] P. Giannozzi, O. Andreussi, T. Brumme, O. Bunau, M. Buongiorno Nardelli, M. Calandra, R. Car, C. Cavazzoni, D. Ceresoli, M. Cococcioni, N. Colonna, I. Carnimeo, A. Dal Corso, S. de Gironcoli, P. Delugas, R. A. DiStasio, A. Ferretti, A. Floris, G. Fratesi, G. Fugallo, R. Gebauer, U. Gerstmann, F. Giustino, T. Gorni, J. Jia, M. Kawamura, H.-Y. Ko, A. Kokalj, E. Küçükbenli,

- M. Lazzeri, M. Marsili, N. Marzari, F. Mauri, N. L. Nguyen, H.-V. Nguyen, A. Otero-de-la Roza, L. Paulatto, S. Poncé, D. Rocca, R. Sabatini, B. Santra, M. Schlipf, A. P. Seitsonen, A. Smogunov, I. Timrov, T. Thonhauser, P. Umari, N. Vast, X. Wu, and S. Baroni, Advanced capabilities for materials modelling with Quantum ESPRESSO., *Journal of physics. Condensed matter : an Institute of Physics journal* **29**, 465901 (2017).
- [66] Hybertsen and Louie, Electron correlation in semiconductors and insulators: Band gaps and quasiparticle energies., *Physical review. B, Condensed matter* **34**, 5390 (1986).
- [67] J. Deslippe, G. Samsonidze, D. A. Strubbe, M. Jain, M. L. Cohen, and S. G. Louie, BerkeleyGW: A massively parallel computer package for the calculation of the quasiparticle and optical properties of materials and nanostructures, *Computer Physics Communications* **183**, 1269 (2012).
- [68] M. Rohlffing and S. G. Louie, Electron-Hole Excitations in Semiconductors and Insulators, *Physical Review Letters* **81**, 2312 (1998).
- [69] M. Rohlffing and S. G. Louie, Electron-hole excitations and optical spectra from first principles, *Physical Review B* **62**, 4927 (2000).
- [70] T. Woźniak, P. E. Faria Junior, G. Seifert, A. Chaves, and J. Kunstmänn, Exciton g factors of van der Waals heterostructures from first-principles calculations, *Physical Review B* **101**, 235408 (2020), arXiv:2002.02542.

## ACKNOWLEDGMENTS

The work was supported by Deutsche Forschungsgemeinschaft (DFG). We gratefully acknowledge financial

support of the German Excellence Initiative by MC-QST and e-conversion. This work has been partially supported by the EC Graphene Flagship project and by ANR projects ANR-17-CE24-0030 and ANR-19-CE09-0026. This work was supported by LNCMI-CNRS, members of the European Magnetic Field Laboratory (EMFL). J.K. acknowledges support by the Alexander von Humboldt foundation. K.W. and T.T. acknowledge support from the JSPS KAKENHI (Grant Numbers 19H05790, 20H00354 and 21H05233).

## AUTHOR CONTRIBUTIONS

A.H., J.K., J.J.F., A.W.H., and A.S. conceived and designed the experiments. T.A, G.C., D.H., and S.R. performed the DFT-GW and BSE calculations. S.R., J.K. prepared the sample. K.W. and T.T. provided high-quality hBN bulk crystals. A.H., A.S., T.P., A.D., C.F., J.K. and K.B. performed the optical measurements. A.H. analyzed the data. C.K., M.P. and C.F. contributed interpreting the data. A.H. and A.S. wrote the manuscript with input from all coauthors.

## COMPETING INTERESTS

The authors declare no competing interests